TU Delft

Delft University of Technology

Data-driven model to predict burst pressure in the presence of interacting corrosion pits

Yarveisy, Rioshar; Khan, Faisal; Abbassi, Rouzbeh

DOI
10.1016/j.jpse.2023.100146

Publication date
2024

Document Version
Final published version

Published in
Journal of Pipeline Science and Engineering

Citation (APA)
Yarveisy, R., Khan, F., & Abbassi, R. (2024). Data-driven model to predict burst pressure in the presence of interacting corrosion pits. *Journal of Pipeline Science and Engineering*, *4*(1), Article 100146. https://doi.org/10.1016/j.jpse.2023.100146

Important note
To cite this publication, please use the final published version (if applicable).
Please check the document version above.

Copyright
Other than for strictly personal use, it is not permitted to download, forward or distribute the text or part of it, without the consent of the author(s) and/or copyright holder(s), unless the work is under an open content license such as Creative Commons.

Takedown policy
Please contact us and provide details if you believe this document breaches copyrights.
We will remove access to the work immediately and investigate your claim.

This work is downloaded from Delft University of Technology.
For technical reasons the number of authors shown on this cover page is limited to a maximum of 10.

Journal of Pipeline Science and Engineering 4 (2024) 100146

Contents lists available at ScienceDirect

Journal of Pipeline Science and Engineering

journal homepage: www.keaipublishing.com/en/journals/journal-of-pipeline-science-and-engineering/

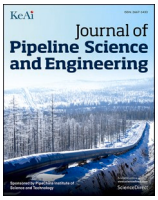

Data-driven model to predict burst pressure in the presence of interacting corrosion pits

Rioshar Yarveisy [a,b], Faisal Khan [c,*], Rouzbeh Abbassi [d]

[a] Centre for Risk, Integrity, and Safety Engineering (C-RISE), Faculty of Engineering and Applied Science, Memorial University of Newfoundland, St. John's, NL, A1B 3X5, Canada
[b] Faculty of Technology, Policy and Management, Safety and Security Science Group (S3G), TU Delft, Delft, 2628BX, the Netherlands
[c] Mary Kay O'Connor Process Safety Center, Artie McFerrin Department of Chemical Engineering, Texas A&M University, College Station, TX, USA
[d] School of Engineering, Faculty of Science and Engineering, Macquarie University, Sydney, NSW 2109, Australia

ARTICLE INFO

Keywords:
Pitting corrosion
Failure analysis
Extreme value analysis
Monte Carlo simulation
Inline inspection
Pipeline failure analysis

ABSTRACT

This paper presents a data-driven approach to predict the pipelines' corrosion-induced Burst failure. In this approach, different aspects of pit growth progression and spatial distribution of pits are simulated. The proposed approach takes advantage of population characteristics to model these aspects of the degradation paths for each pipe section down to the size of single joints. The insights obtained from simulations are used to project the degradation of each pipe section. Understanding corrosion behavior and field data are used to model the corrosion-related parameters such as corrosion pit dimensions, probability and time of initiation, and location. The failure is modeled using the probabilistic simulation considering degradation rate, interactions among pits, and material properties as stochastic variables. The proposed approach and included models are tested using multiple real-life inline inspection datasets. Validation of predicted properties shows prediction errors ranging from 3%–10% depending on the three remaining strength calculation approaches. This work aimed to serve as an important tool for risk-based maintenance prioritization, inspection interval assessment, and the fitness of service assessment of pipelines.

1. Introduction

Pipelines are the safest, most reliable means for transporting fluids, whether raw materials or products. The pipeline failures may lead to catastrophic consequences, thus demanding diligent integrity management programs (IMP). The IMPs are risk management programs with continuous improvement and self-assessment provisions (API, 2019). Risk management programs comprise risk analysis and control (Khan et al., 2021a). Risk analysis involves hazard identification, probability estimation, and consequence assessment.

Hazards posing threats to oil and gas pipelines could be divided into three categories (ASME, 2018): (1) time-dependent, (2) time-independent or random, and (3) potentially time-dependent. Corrosion damage is the most common time-dependent cause of pipeline incidents and accidents, except for some sectors where third-party damage is the most cited cause (PHMSA, 2021). Consequently, developing viable predictive degradation models is necessary for pipeline risk assessment. Such models rely on historical inspection data to infer possible degradation paths in the future. From an integrity management point of view, degradation models can be applied to optimize inspection intervals, prioritize maintenance actions, or manage resources.

Over the past decades, operators have increasingly relied on non-destructive testing (NDT) and especially inline inspection (ILI) tools to monitor the condition of their assets. ILI tools are used to detect and measure pipeline anomalies. Anomalies or features are any deviations from the initial and ideal shape of the line pipe or its surface characteristics. From an integrity management perspective, the data obtained from ILI inspections are used to assess the current state of the asset or to predict possible degradation progress using historical data (Xie and Tian, 2018). Consecutive ILI datasets are valuable assets in predicting corrosion progress through statistical analysis (Alamilla and Sosa, 2008; Dann and Maes, 2018; Nessim et al., 2009; Sánchez et al., 2012) or probabilistic approaches such as Bayesian inference (Adumene et al., 2020; Heidary and Groth, 2021) or Markov chains (Valor et al., 2013), and subjective fixed corrosion rates or power law corrosion models (Tak and Kim, 2018).

* Correspondence author.
E-mail address: fikhan@tamu.edu (F. Khan).

https://doi.org/10.1016/j.jpse.2023.100146
Received 20 May 2023; Received in revised form 17 August 2023; Accepted 17 August 2023
Available online 19 August 2023
2667-1433/© 2023 The Authors. Publishing Services by Elsevier B.V. on behalf of KeAi Communications Co. Ltd. This is an open access article under the CC BY license (http://creativecommons.org/licenses/by/4.0/).

One of the failure modes associated with corroded pipelines is burst, where the degradation progress impairs the pipeline's integrity until it cannot contain the pressure, resulting in a long break in the pipe. Hence, the pipeline's operational and maximum allowable pressure should be revised according to its remaining strength throughout the service life. Many standards and research articles have relied on experimental and numerical simulations to provide deterministic approaches for burst pressure assessment of pipelines (Ossai et al., 2015). Deterministic burst pressure assessment approaches require information on the dimensions of corrosion pits and the line pipe in addition to its material characteristics (ASME, 2012; CSA, 2019; DNV, 2019). These methods also include the impact of interacting corrosion pits in calculating the impaired pipe's pressure. Flaw interaction occurs when two or more corrosion pits are in each other's vicinity in a way that the failure pressure is less than the failure pressure expected from individual features in the cluster (ASME, 2012).

Assessing pipeline burst pressure requires multiple parameters, including line pipe dimensions and mechanical characteristics and the dimensions of the corrosion pits. From a predictive perspective, in addition to the depth growth, degradation progress in other dimensions should also be modeled. Moreover, including the impact of interacting corrosion pits requires the model to include pit initiation. The uncertainty involved with all aspects of corrosion-related phenomena from pit initiation to location, growth, and passivation requires the use of probabilistic or stochastic approaches to capture the possible paths degradation progress might follow.

This work puts forward a data-driven model approach for the predictive assessment of burst pressure relying on corrosion pit population trends inferred from multiple consecutive ILI reports. The method uses contemporary stochastic degradation models integrated with probabilistic simulation to simulate pipeline external surface degradation progress. The simulation approach is adopted to monitor possible degradation paths and reduce the uncertainty of new corrosion pits' initiation and integration with preexisting defects. Supported by the results presented here, this approach, by providing accurate joint-wise insights, could contribute to operational costs in addition to operational safety. This is due to location accuracy's significant role in minimizing downtime and maintenance costs (Tan and Kramer, 1997; Vassiliadis and Pistikopoulos, 2001).

This article uses a seven-year-long ILI dataset comprising four inspection reports of more than 3 km of buried crude transmission large-diameter cross-country pipeline to calibrate and validate the proposed method. The first three reports are used to inform the degradation models, and the fourth report is used to assess the accuracy by comparing the predicted burst pressures for individual pipe joints with the measurements. The results show great agreement between the predictions and measurements, with maximum prediction errors ranging 2%–6 % over the two-year time horizon depending on the burst pressure assessment method.

2. Methodology

The data-driven methodology to develop predictive burst pressure of pipelines is presented in Fig. 1. The developed methodology comprises four distinct steps. The first step, data processing, will be discussed in some detail when exploring the case study in Section 3. As illustrated in the figure, the complete dataset is used to model time-dependent variables. The most recent inspection report is used for stationary parameters and the initial condition for the Monte Carlo simulation (MCS). The second step comprises modeling degradation parameters required for burst pressure assessment where: (1) Pit depth growth is modeled using extreme value analysis (EVA); (2) Pit nucleation is modeled using homogeneous Poisson process (HPP); (3) Spatial distribution of pits is simulated using uniform distributions; (4) Feature dimensions are simulated using Weibull distribution of pit length to depth ratios of the most recent inspection report.

After obtaining the parameters required for degraded surface simulation, MCS models multiple instances of each pipe joint in step three. MCS is adopted to capture the possible degradation paths occurring due to the interaction among the stochastic parameters. The burst pressure for each instance of each pipe joint is then calculated using three standards, DNV-RP-F101 (DNV, 2019), ASME B31G (ASME, 2012), and CSA Z662 (CSA, 2019) in step four. These three approaches are selected due to their distinct pit interaction rules or burst pressure assessment formulations. This section discusses each component of the workflow in more detail.

2.1. Stochastic degradation model

2.1.1. Pit depth growth rate

Corrosion is a stochastic phenomenon. Two stochastic aspects of localized corrosion progress are pit depth growth and re-passivation. The growth rate varies significantly among corrosion pits on a surface, and defects that have reached stable or super-stable states grow consistently and pose a greater threat to structural integrity. Melchers et al. (2008a) suggest that approximately one-third of corrosion pits reach these stages, and the rest remain meta-stable or passivate and go dormant. Here, this principle is applied by assigning growth to one-third

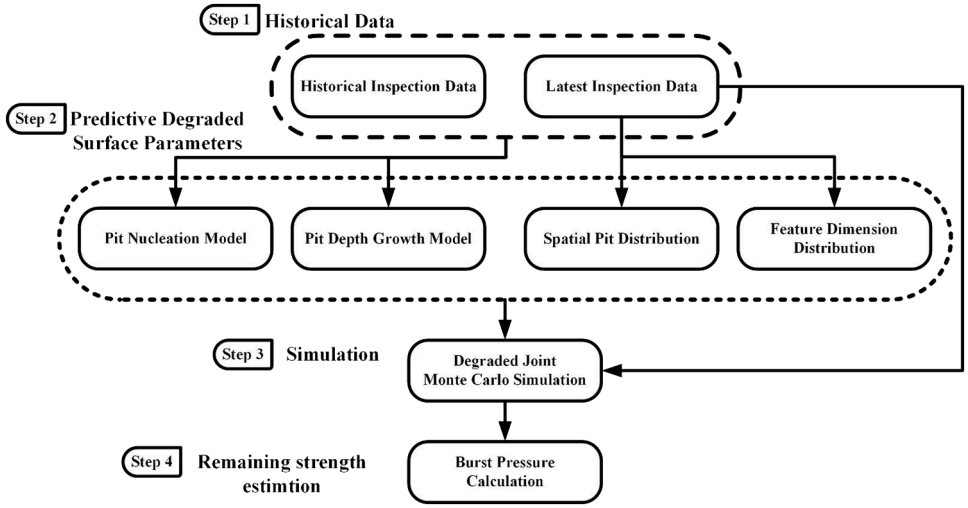

Fig. 1. Overview of predictive burst pressure assessment methodology.

of features on the surface in each simulated instance.

Considering the stochasticity of corrosion processes, many choose to model degradation progress based on population trends (Dann and Maes, 2018; Gomes et al., 2013; Gong and Zhou, 2018; Heidary and Groth, 2021). Contrary to this population-based approach, this work models pit depth growth based on the trends observed in population outliers, i.e., pits with maximum depth on each section. Furthermore, burst pressure assessment and pit unification methods for interacting pits rely on the maximum depth observed in complex-shaped features. Hence, focusing on accurate modeling of outlier population growth helps develop a more safety-oriented assessment of degradation progress. Even though conservative for the whole population, this serves the prediction viability by focusing on the most threatening defects.

EVA is a branch of statistics focused on population outliers. This work utilizes extreme value theory to describe the behavior of population outliers and uses the distribution parameters to model their time-dependent trends.

EVA. Statistical analysis of pits with outlier depth is a long-established application of EVA, with the first known instance dating back to the 1950s (Aziz, 1956). Many researchers have utilized EVA to study pit depth variability in the marine environment (Melchers, 2004; 2005a; 2005b), on buried pipelines (Alfonso et al., 2010; Valor et al., 2010; Velazquez et al., 2009; Velázquez et al., 2009), and laboratory experiment results (Rivas et al., 2008). Moreover, EVA-based approaches have been used to extrapolate direct inspection results for risk assessment of unpiggable pipelines (Alfonso et al., 2010; Valor et al., 2007) and predict the non-stationary behavior of the extrema (Scarf, 1992; Yarveisy et al., 2022).

EVA comprises many techniques ranging from frequentist distribution-based approaches to Bayesian inference-based methods (Coles et al., 2001). This work adapts the block maxima (BM) approach to describe the observed local maxima by fitting them to a generalized extreme value (GEV) distribution. The distribution parameters are then used to model the time-dependent behavior of maxima from each time-step using linear regression. This approach shown in Fig. 2 permits predicting the distribution of local maxima depths based on historical data.

The implemented approach (1) divides the dataset into separate inspection runs, (2) further divides the reports by grouping the pits detected on each pipe joint, (3) filters out all observations on each joint (block) except the maximum, (4) fits the population of local maxima to the GEV distribution (Gumbel distribution in this work) (Dey and Yan, 2016), and (5) obtains a linear model for each distribution parameter using regression analysis to predict distribution parameters.

The population of local extrema can be described using the GEV family of distributions. GEVs are the limiting distribution of sample extrema of independent identically distributed (i.i.d.) random variables (Kotz and Nadarajah, 2000). Eq. (1) illustrates the general form of the GEV family of distributions where $\xi = 0$ represents the GEV Type-I, the Gumbel distribution.

$$G(x) = \exp\left\{ -\left[1 + \xi\left(\frac{x-\mu}{\sigma}\right)\right]^{-\frac{1}{\xi}}\right\},\ -\infty < \mu,\ \xi < +\infty,\ 0 < \sigma \tag{1}$$

Where ξ is the Gumbel distribution shape, μ is the Gumbel distribution location, and σ is the Gumbel distribution scale.

Some researchers suggest using the Fréchet distribution for pits with maximum depth. (Melchers, 2008b).Other studies show that the BM approach is deficient, and it is best to model pits with extreme depth using more advanced EVA approaches (Rivas et al., 2008; Yarveisy et al., 2022). But in most cases, the maximum pit depths are fitted to a Gumbel distribution. This work adopts the Gumbel distribution to simulate pit depth growth based on the local maxima due to its convenience and sufficient accuracy. Eq. (2) shows the cumulative distribution function of the Gumbel distribution.

$$G(x) = \exp\left[-\exp\left(\frac{x-\mu}{\sigma}\right)\right],\ -\infty < x < +\infty \tag{2}$$

Non-stationary distribution modeling. Granted that pitting corrosion is a temporal phenomenon, the distribution of pit depths, and consequently, pits with extreme depth vary by time. When the population characteristics change over time, they are called non-stationary processes. It was mentioned that distribution parameters are used to model growth and predict population behavior. The non-stationary behavior of GEV distributed observations can be modeled using their distribution parameters (Coles et al., 2001). This approach transforms the stationary distribution of eq. (2) to the time-dependent Gumbel distribution shown in Eq. (3).

$$G_x(t) = \exp\left\{ -\exp\left[\frac{x-\mu(T)}{\sigma(T)}\right]\right\},\ -\infty < x < +\infty \tag{3}$$

Where the time-dependent location $\mu(T)$ and scale $\sigma(T)$ are obtained from linear regression of individual Gumbel distribution parameters at each time-step to the general form of Eq. (4) below.

$$y = aT + b \tag{4}$$

Pit depth growth modeling and simulation. As shown in Fig. 1, the surface degradation models are used in the MCS of surfaces. The pit growth degradation model utilizes the distribution parameters predicted at the desired time. The growth rate assessment for each instance of the MCS is done by (1) drawing from the predicted distribution, (2) assessing the growth rate by comparison with the pit with maximum depth on individual pipe joints of the most recent report, and (3) assigning the growth rate randomly to one-third of pits on that pipe joint and obtaining their respective depths at the desired time. This includes both newly initiated and existing pits. The pseudocode used to simulate growths is presented in Fig. 3 below. Each pipe joint's growth rate is simulated using the population of extreme pit depths observed in historical data. Each joint's degradation paths are simulated using its latest inspection data as the initial condition.

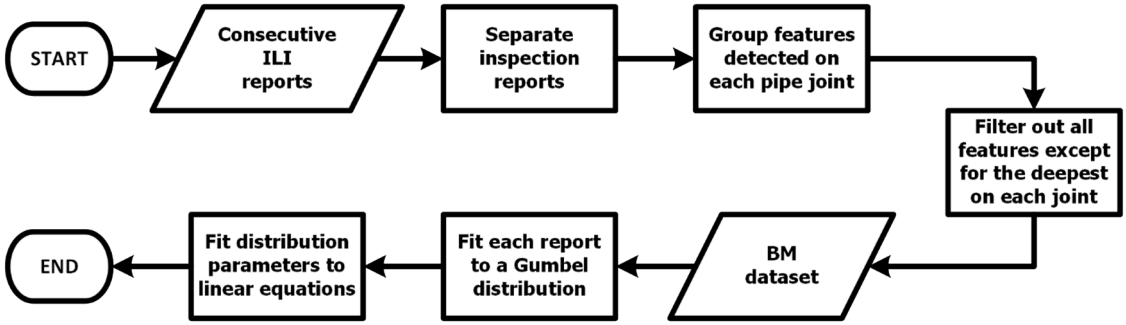

Fig. 2. The workflow for predictive corrosion depth model using BM and GEV distribution.

Pit depth growth rate function:

Pass In: predicted Gumbel distribution paramters, latest inspection report, time horizon

Each joint's max. depth at desired time = draw one from Gumbel distribution with parameters predicted at the desired time.

Each joint's annual growth rate = (each joint's max. depth at desired time – each joint's max. depth at latest inspection) / time horizon

While Each joint's annual growth rate is less than zero

Each joint's max. depth at desired time = draw one from Gumbel distribution with parameters predicted at the desired time.

Each joint's annual growth rate = (each joint's max. depth at desired time – each joint's max. depth at latest inspection) / time horizon

End while

Pass Out: Each joint's growth rate

Fig. 3. Pseudocode for Joint-wise pit depth growth rate assessment function.

2.2. Pit initiation

The importance of pit initiation is due to its impact on pit density on the surface. Pit density plays an important role in the severity and probability of interaction among pits and, subsequently, load distribution and burst pressure (Shekari et al., 2016). In low alloy and mild steels, in the absence of a passive protective film, the localized corrosion process is initiated when the electrical potential between two zones is high enough to provide the required driving force for electron flow (Melchers, 2015). Considering numerous anodic and cathodic sites on exposed surfaces of metallic assets, oxygen, and electrolytes, the time to initiation of corrosion pits is highly uncertain.

Multiple studies have shown that the time to initiation of corrosion pits follows an exponential distribution, leading to an HPP to simulate this phenomenon (Heidary and Groth, 2021; Shibata, 1996; Tsukaue et al., 1994; Zhou et al., 2017). On the other hand, some have adopted a non-homogeneous Poisson process (NHPP) to model pit initiation times over long periods (Zhang et al., 2012; Zhang and Zhou, 2014). NHPP application is motivated by the need to reflect changing initiation rates observed in long-term corrosion tests and field data. Here, an HPP approach is used to describe this parameter as the time horizon is short, and it is assumed that the changes over short periods are linear enough to be represented using a constant rate.

2.2.1. Homogeneous Poisson process (HPP)

The pit densities per square meter obtained from consecutive ILI datasets follow non-stationary Weibull distributions (Khan et al., 2021b). A predictive approach to assess pit densities in desired time is utilized to estimate the HPP rate function. First, pit densities on each pipe joint are fitted to a Weibull distribution. The distribution parameters are used to obtain a time-dependent Weibull distribution using linear regression, similar to the procedure discussed in Section 2.1.1.2 *Non-stationary distribution modeling*. Eq. (5) below shows the time-dependent Weibull distribution, where $\kappa(t)$ and $\lambda(t)$ are the time-dependent shape and scale parameters. The time-dependent parameters are obtained from linear models of respective parameters fitted to each report's pit densities per square meter.

$$\begin{cases} 1 - e^{-\left(\frac{x}{\lambda(t)}\right)^{\kappa(t)}}, & x \geq 0 \\ 0, & x = 0 \end{cases} \tag{5}$$

Pit densities on individual pipe joints are drawn at the desired time in the future, using the time-dependent Weibull distribution. The initiation rate for each pipe joint is assessed compared to the number of pits identified in the most recent inspection run. This value is converted to density per square meter based on the joint's dimensions. The mean of the generated pits in the interval is taken as the initiation rate at that time interval. The steps are repeated using MCS to capture possible variations. The mean of the initiation rates in the time interval is used to assess the initiation function of the HPP using linear regression. Fig. 4 shows the approach for evaluating the initiation rate for the HPP simulation of pit initiation on each pipe joint.

2.2.2. Pit initiation simulation

Using the estimated generation rate, pit initiation on each pipe joint is simulated using the time horizon and the area surface of the joint. This method assesses the number of generated pits using a draw from a Poisson distribution during the time interval. The time of initiation is simulated using draws from a uniform distribution. Paupathy (2010) discusses the simulation approach applied here in more detail. The pseudocode of Fig. 5 describes the function used for simulating pit initiation on each pipe joint used in the MCS.

2.3. Pit dimensions and spatial distribution

The data has shown no time-dependent behavior or a discernible trend when concerned with the length of the corrosion pit to depth ratios. Khan et al. (2021b) present this parameter using Weibull distributions. The pit length to depth ratio is simulated using draws from a Weibull distribution with parameters fitted to the latest inspection report. Furthermore, the simulated pit shapes are idealized as conical defects, i.e., the pit length and width are equal.

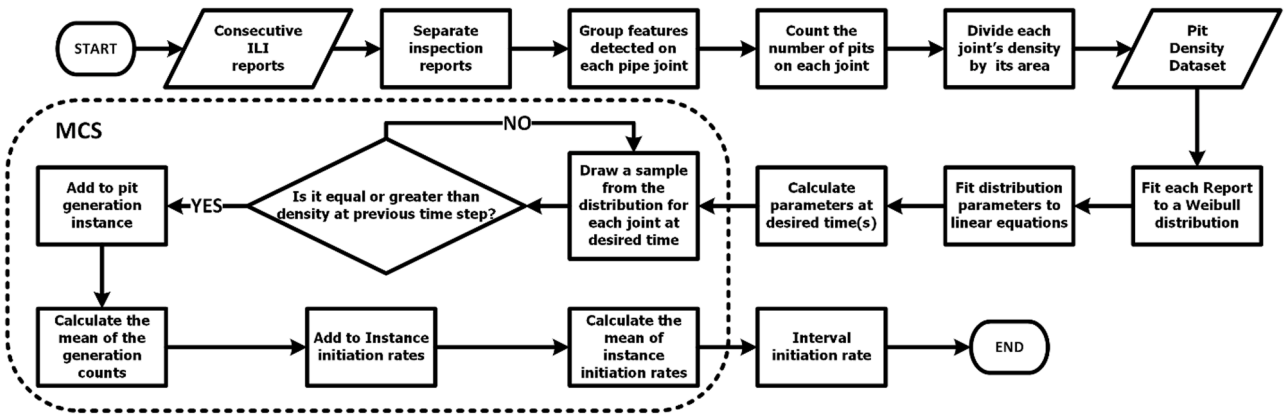

Fig. 4. The initiation rate assessment methodology.

Feature initiation function

Pass In: time horizon, joint area, initiation rate

Number of generated pits = draw one from Poisson distribution where rate = initiation rate * time horizon

Time of generation = draw "Number of generated pits" from uniform distribution with minimum of zero and maximum equal to timee horizon and sort it in ascending order

Pass Out: Times to initiation

Fig. 5. Pseudocode for HPP pit initiation simulation.

Another stationary parameter is the pit distribution over the surface. Experimental results and field data suggest pit location to be a random process, showing no discernible trends on large enough surfaces (Cawley and Harlow, 1996; Melchers, 2010). On the other hand, field inspection results suggest varying trends depending on the environment, application, and corrosion protective measures (Khan et al., 2021b; Larrosa et al., 2018). The simulated corrosion pits are placed using draws from a uniform distribution with axial and angular locations calibrated to individual pipe joints' dimensions.

2.4. Probabilistic (Monte Carlo) simulation

Monte Carlo (MC) simulation with many variations sampling is the most widely used probabilistic simulation technique. The method relies on sampling from distributions multiple times or simulating processes for long enough durations to obtain information on parameters of interest using the law of large numbers or other inference methods (Kroese et al., 2014). MC methods are used to handle two problems: probabilistic and deterministic. MC methods are used to observe random numbers chosen to represent the random physical processes, providing the information required to infer their interaction. This approach to direct simulation of probabilistic problems is the simplest form of MC methods (Hammersley and Handscomb, 1964).

The MCS approach implemented here uses the predicted distributions of the parameters, i.e., maximum pit depth, pit initiation function, pit length, and spatial distribution of corrosion pits to simulate various degradation paths. The degraded pipe surface is simulated by superposing the newly generated corrosion pits on the surface with characteristics obtained from the latest inspection. The degradation progress is simulated by increasing the depth and assigning dimensions to pits. An overview of the approach to simulate the degraded pipe surfaces is presented in Fig. 6. The functions related to previously presented parameters are included without any detail and by their name.

2.5. Burst pressure assessment models

2.5.1. DNV RP F101 (DNV, 2019)

According to RP-F101, pit interaction is assessed using the axial and circumferential location of corrosion pits and the pipe's external nominal diameter and wall thickness. Based on these criteria, corrosion pits with an axial distance of 2.5 $\sqrt{Dt}$ and circumferential separation of less than 360 $\sqrt{t/D}$ degrees are interacting, in which t is the pipe wall thickness and D is the nominal external diameter. In this approach, overlapping corrosion pits form a complex defect with a depth equal to the deepest pit. The length of the complex defect is assessed to reflect the combined length of all overlapping defects.

Fig. 7(a) illustrates the procedure to combine the overlapping corrosion pits located at each other's vicinity according to the circumferential distance rule mentioned above. Following the unification of overlapping pits, the impact of groups of defects that satisfy the interaction distance criterion on the burst pressure is assessed. The minimum allowable pressure due to different grouping of interacting pits is used as the burst pressure of the pipe section. Fig. 7(b) illustrates the procedure to construct these groups.

To assess the burst pressure by including the impact of interacting pits, the original equation is simplified as shown in Eq. (6), where t is the

```
MCS
    Pass In: Number of simulations, Predicted Gumbel parameters, Predicted generation rate, Predicted Weibull length to depth ratio parameters, Most recent inspection report, Pit initiation function, Pit depth growth function
    For i in 1 to Number of pipe joints
        Calculate joint surface area
        Assess growth rate using "Pit depth growth function"
        Assess number of initiated features and their time of initiaion using "Pit initiation function"
        Assign location to the generated pits by:
            Draw from uniform distribution between 0-359
            Draw from uniform distribution between 0-pipe joint length
        Add the new to the existing pits from most recent report
        Select one-third of pits on the surface randomly
        If newly generated
            Assign pit length and width by
                Drawing one from length to depth ratio Weibull distribution and assign to both
            Assign depth by
                Growth rate × (time horizon – time of initiation)
        Else
            While length less than the most recent report
                Assign pit length and width by
                    Drawing from length to depth ratio Weibull distribution
            Assign depth by
                Growth rate × time horizon
    Pass out: Updated pit list
```

Fig. 6. MCS of degraded surface pseudocode.

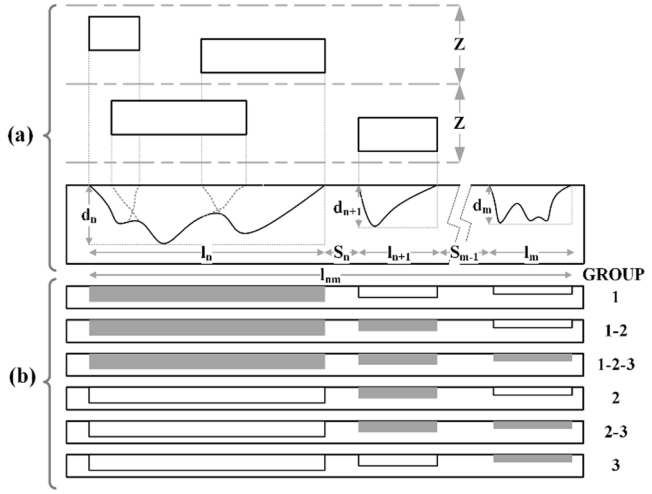

Fig. 7. Overview of (a) overlapping pit combination and (b) assessing the minimum burst pressure of a group of interacting pits, adapted from RP-F101 (DNV, 2019).

nominal pipe wall thickness and d_{nm} is the depth of the combination of defects, and both safety factors are set to one ($\gamma_m = \gamma_d = 1$). Length correction factor Q_{nm} is calculated according to Eq. (7) and parameters pit length l_{nm} and pit depth d_{nm} are obtained using Eq. (8). Fig. 7(b) illustrates how the parameters are obtained from the data concerned with corroded regions.

$$p_{nm} = \gamma_m \frac{2\ tf_u\left[1-\gamma_d\left(\frac{d_{nm}}{t}\right)^*\right]}{(D-t)\left[1-\frac{\gamma_d\left(\frac{d_{nm}}{t}\right)^*}{Q_{nm}}\right]} = \frac{2\ tf_u\left[1-\left(\frac{d_{nm}}{t}\right)\right]}{(D-t)\left[1-\frac{\left(\frac{d_{nm}}{t}\right)}{Q_{nm}}\right]},\ n,m=1,\cdots,\ N \tag{6}$$

$$Q_{nm} = \sqrt{1+0.31\left(\frac{l_{nm}}{\sqrt{Dt}}\right)^2} \tag{7}$$

$$\begin{cases} l_{nm} = l_m + \sum_{i=n}^{m-1} l_i + s_i,\ n,m=1,\ \cdots,\ N \\ d_{nm} = \frac{\sum_{i=1}^{m} d_i l_i}{l_{nm}} \end{cases} \tag{8}$$

Where s is the distance between adjacent pits.

2.5.2. ASME B31G (ASME, 2012)

B31G follows a distance-based interaction assessment criterion based on wall thickness. Defects closer than three times the nominal pipe wall thickness in both axial and circumferential directions are considered interacting. All interacting pits should be unified and considered one, where the depth is equal to the maximum depth among all defects. The length of the combined defect is assessed by reflecting it on a line parallel to the pipe's longitudinal axis. Fig. 8 below shows the pit interaction criteria and pit unification according to guidelines provided by this standard.

This article assesses the burst pressure using the level 1 evaluation procedure and the modified B31G formulation according to Kiefner and Vieth (1989, 1990), where the burst pressure is calculated using Eq. (9). Where, S_F is the failure stress that can be calculated using Eq. (10), p_F is the failure pressure, and M is the bulging stress magnification factor and S_{flow} is the flow stress. M can be calculated using Eqs. (12) and (13), where z is a parameter dependent on pipe dimensions and defect length, calculated as $z = L^2/Dt$, where L is the pit length. Flow stress for carbon steel pipelines operating below 120°C can be calculated using Eq. (11), where specified minimum yield strength (SMYS) is at ambient conditions. Flow stress cannot exceed the specified minimum tensile strength (SMTS) of the pipe.

$$p_F = 2\ S_F t/D \tag{9}$$

$$S_F = S_{flow}\left[\frac{1-0.85(d/t)}{1-0.85(d/t)/M}\right] \tag{10}$$

$$S_{flow} = 1.1\ \text{SMYS} \tag{11}$$

$$M = \left(1 + 0.6275\ z - 0.003375\ z^2\right)^{0.5},\ z \le 50 \tag{12}$$

$$M = 0.032\ z + 3.3,\ z > 50 \tag{13}$$

2.5.3. CSA Z662 (CSA, 2019)

The approach adopted by this standard is similar to that of B31G, with different interaction criteria, whereas the distance is increased to six times (6 t) the pipe wall thickness compared to three times (3 t) discussed in B31G above.

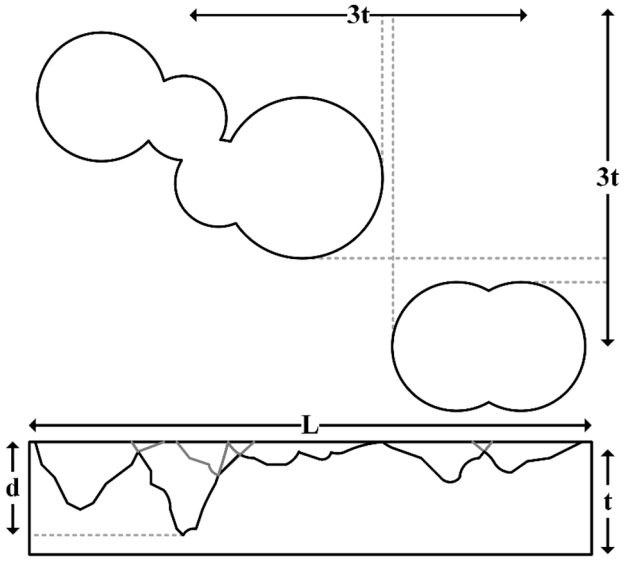

Fig. 8. Interaction criteria and pit unification approach adapted from B31G (ASME, 2012).

3. Testing and application of the approach and models

This section present the case study that utilizes the data from four consecutive ILI runs obtained using magnetic flux leakage (MFL) tools over seven years. The dataset is obtained from sections with the minimal repair of more than 200 km of 32 inches buried cross-country crude carrying pipeline. The first two inspection runs are conducted using the same, and the third and fourth inspections each use a different generation of MFL technology. The data provider has not shared other information about the asset. Khan et al. (2021b) provide a detailed analysis of the data and the raw dataset used in this study. This section briefly discusses the steps implemented to infer the required parameters used in the MCS of the pipeline degradation.

When discussing corrosion, the term "pitting" could be a source of dispute among researchers (Melchers, 2015). Some believe that pitting corrosion should only apply to highly localized corrosion of metals with passive films, e.g., stainless steel or aluminum (Uhlig and Revie, 1985). Subsequently, rendering the application of the terminology related to pitting corrosion inappropriate for metals with insignificant or no passive film, e.g., low alloy and mild steels. Here, the more classical point of view, in line with highly influential corrosion research, is adopted, where the term is applied to metals with or without passive films alike (Burstein et al., 2004; Butler et al., 1972; Mercer and Lumbard, 1995).

The metal loss features identified using NDT and MFL tools are categorized based on their geometry and dimensions. Here, corrosion pits are identified using Eq. (14) (POF, 2021), where A is equal to pipe wall thickness for $t \ge 10$ (mm) and $A = t$ for pipes with nominal wall thickness greater than 10 mm. This equation, w and l are the corrosion feature's width and length.

$$(A \le (w \wedge l) \le 6\ A\ ) \wedge \left(0.5 < \frac{l}{w} < 2\right)\ ! \wedge ((w \wedge l) \ge 3\ A) \tag{14}$$

The original dataset comprises 86,384 external corrosion features on 267 joints extended over 3.2 km of line pipe. The dataset is reduced to 16,240 observations located on 246 pipe joints, with a length of 3 km, according to Table 1.

The first three inspection reports are used to develop degradation models and extract parameters required for the MCS of individual pipe joints. The simulation is conducted to assess degradation at year seven, and it is validated with the state of asset obtained from the last inspection run. Each pipe joint is presented using its impaired maximum allowable pressure. Maximum allowable pressure equals the minimum burst pressure calculated on each pipe joint. In addition to degraded surface characteristics, burst pressure assessment requires line pipe dimensions and mechanical characteristics. Here, absolute values, according to Table 2, are utilized instead of a stochastic representation of these characteristics.

Table 1
Tally of corrosion pits.

Year	Pit count
1	2,704
3	2,945
5	4,192
7	6,399

Table 2
Line pipe dimensions and mechanical properties.

SMTS (MPa)	SMYS (MPa)	External diameter (mm)	Wall thickness (mm)
435.06	317	810	7.1

4. Results and Discussion

The dataset above is used to estimate the stochastic parameters required as inputs to the MCS of degraded surfaces. Here, the first three inspection reports are used to infer the parameters, and the seventh inspection run is used to validate the model. This section first explores the data used for calibration of the simulation scheme for depth growth, pit initiation, spatial distribution, and dimensions based on the data. The simulation results and comparison with the asset state are discussed last.

4.1. Pit depth growth

The approach used to assess the growth trend among corrosion pits with maximum depth on each section was discussed under Section 2.1.1. Fig. 9(a) and (b) illustrate the distribution and the quantiles of the pit depths in each year. The density plots of the first and second reports demonstrate growing means, flatter peaks, and fatter tails, suggesting a growing population. Contrary to the expectation for the third and fourth reports to have the same trend, they show lower means and less significant tails. This issue is tied to changes in inspection technology resulting in the detection of shallower features and the impact of clustering algorithms (Khan et al., 2021b).

After filtering out all observations but features with maximum depth on each pipe joint, the density plots and quantiles of Fig. 10 show more consistent trends. Fig. 9(a), the local maxima show an improved trend in their tail area and peaks. The population means and increased outliers also show improved trends, as illustrated in Fig. 10(b).

The BM dataset is then used to estimate linear models of the location and scale parameters of the Gumbel distribution. The linear regression of the distribution parameters is conducted using the first three report's BM fitted to Gumbel distributions using maximum likelihood estimation. Table 3 shows the Gumbel distribution parameters and their associated standard errors resulting from fitting the maximum pit depths on each pipe joint.

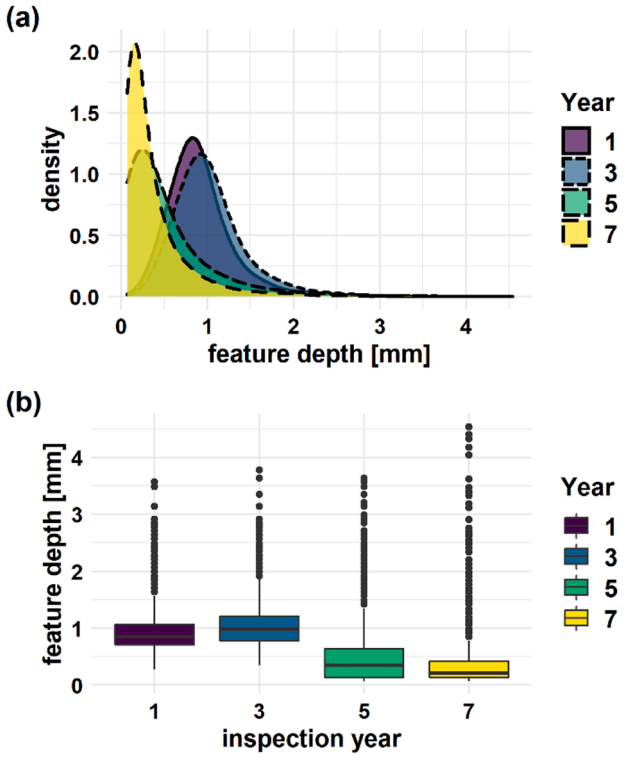

Fig. 9. (a) density plots and (b) box plots of population pit depths.

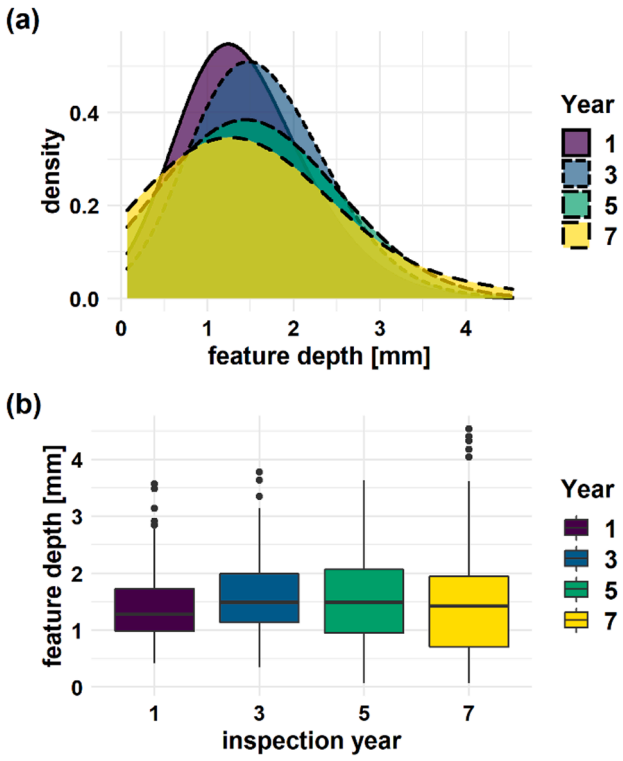

Fig. 10. (a) density plots and (b) box plots of local depth maxima.

Table 3
Gumbel distribution parameters of the fitted BM pit depths.

Year	Location	Location Std. Err.	Scale	Scale Std. Err.
1	1.15	0.031	0.45	0.023
3	1.34	0.033	0.48	0.024
5	1.14	0.046	0.68	0.033

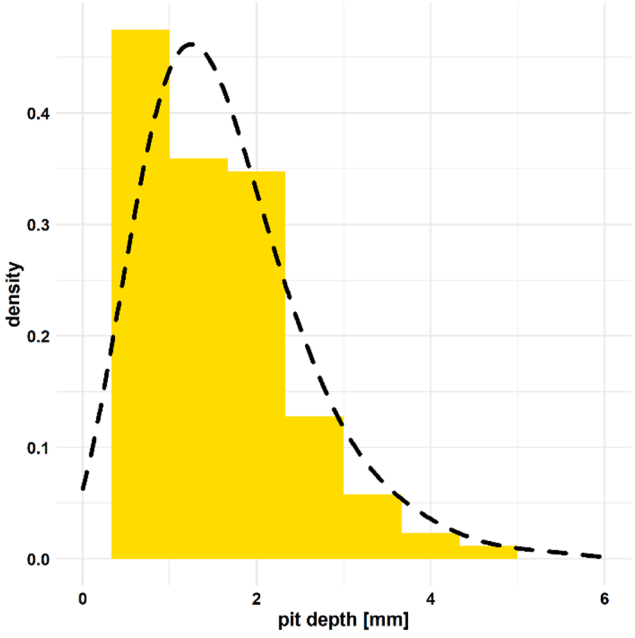

Fig. 11. Seventh-year BM pit depths and predicted Gumbel distribution's density.

The parameters shown in Table 3 are used to obtain Eqs. (15) and (16) for the time-dependent location and scale linear models using linear regression, where T is time in years.

$$\mu(T) = -0.003\ T + 1.22 \tag{15}$$

$$\sigma(T) = 0.06\ T + 0.37 \tag{16}$$

The equations above are used to predict the distribution parameters. In this case, the simulation results will be validated against the state of the asset obtained from the seventh year's inspection report. The predicted seventh-year maximum depth distribution is shown in Fig. 11, where the histogram of the measured BM pit depths at year seven are compared with the density plot of the predicted distribution.

4.2. Pit initiation

An approach like Section 4.1 is used to model the pit densities on pipe joints using Weibull distributions. Each joint's pit densities per square meter are first fitted to Weibull distributions. The parameters of the Weibull distributions at the desired time are predicted using regression analysis of distribution parameters from historical data. MCS is used to simulate the pit densities on pipe joints in the seventh year. By comparing the simulated densities and the pit density per square meter obtained from the fifth-year report, one can assess each pipe joint's initiation rate. The initiation rate for each simulated pipeline instance is calculated using the mean of the individual joint initiation rates. The HPP rate applied for MCS is obtained by averaging the rates obtained from each instance.

Table 4 shows the parameters of the Weibull distributions obtained from fitting the pit densities per square meter of pipe joints as reported in the first three ILI reports. Fig. 12 demonstrates the goodness of fit to the Weibull distribution for pit densities, where the left column compares the histogram of the pit densities according to the data with the theoretical density plot. The right column depicting the theoretical quantiles against the quantiles observed from data also shows good overall agreement, including the extremes with the fit to the Weibull distribution.

Seventh-year pit densities are predicted using the Weibull distribution parameters and linear regression. Eqs. (17) and (18) show the time-dependent shape and scale parameter functions. Table 5 highlights the difference between the predicted and observed Weibull distribution parameters at year 7. Here, contrary to the satisfactory accuracy in

Table 4
Distribution parameters of pit densities per square meter fitted to Weibull distributions.

Year	Shape	Shape Std. Err.	Scale	Scale Std. Err.
1	1.08	0.05	1.81	0.12
3	1.13	0.06	1.99	0.12
5	1.18	0.06	2.80	0.16

Table 5
Comparison of predicted V. estimated Weibull distribution parameters.

Parameter	Predicted	Observed	Std. Err.
Shape	1.23	1.16	0.04
Scale	3.19	4.08	0.45

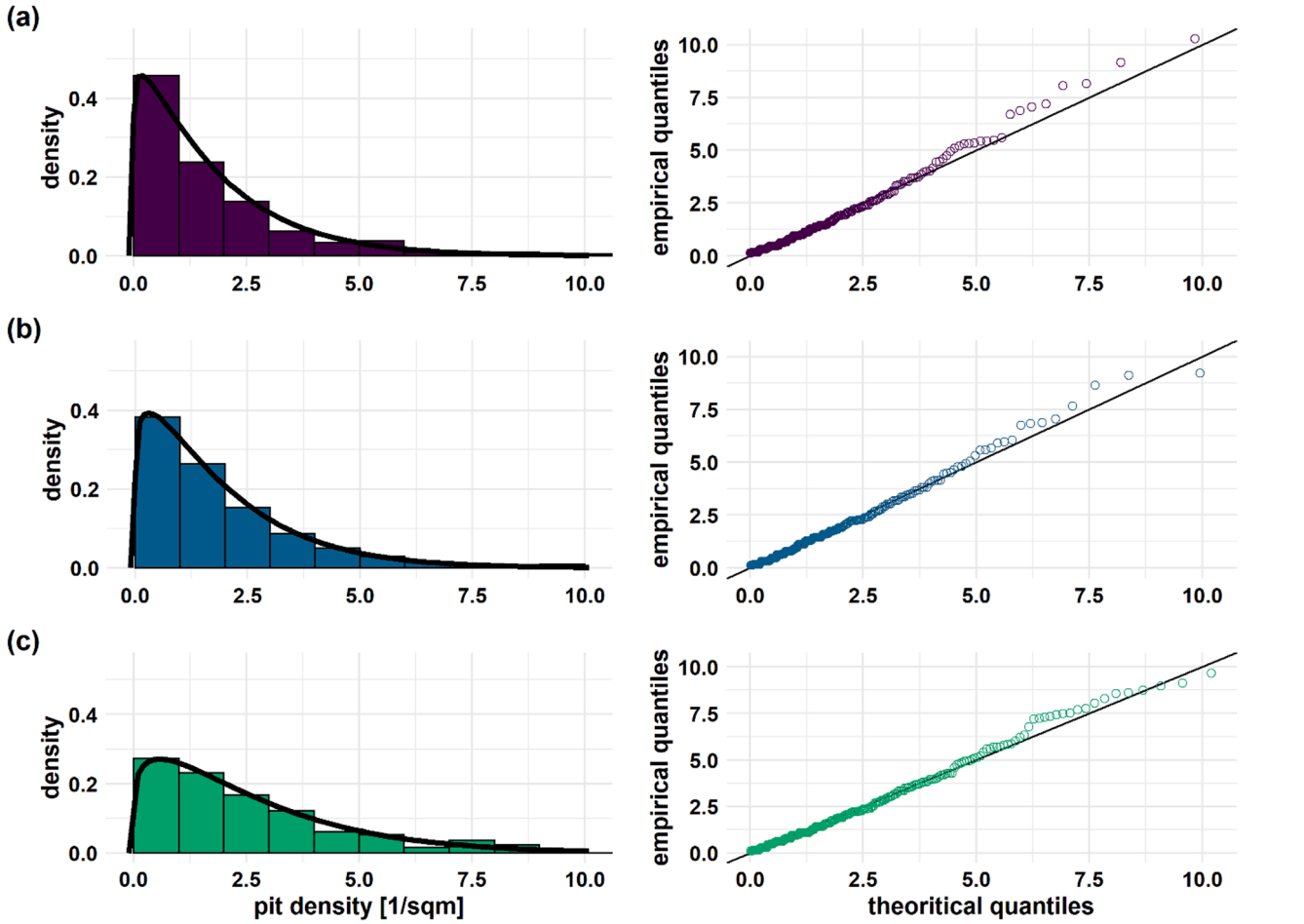

Fig. 12. The goodness of fit plots for pit densities of (a) the first, (b) the third, and (c) the fifth-year reports.

predicting the shape parameter, the prediction error for the scale parameter is significant. The impact of the scale parameter's low accuracy on the predicted distribution emerges as a less significant tail area and, consequently, more density around the distribution mean.

$$\kappa(t) = 0.03\ t + 1.05 \tag{17}$$

$$\lambda(t) = 0.25\ t + 1.46 \tag{18}$$

Using the information obtained above and implementing the MCS discussed in 2.2.2, the HPP rate is estimated as $\lambda_{HPP} = 0.36\ (sqm^{-1})$ for the two-year period.

4.3. Pit dimension and spatial distribution

This article's simulation procedure adopts a pit shape idealization where corrosion pits are imagined to be conical. Consequently, the length and width of the distribution are equal. It has been shown that the corrosion feature-length to depth ratio follows a Weibull distribution (Khan et al., 2021b). Here the same assumption is applied and validated against observations using ILI data. The pit length to depth ratio is the best fit for Weibull distributions. Even though the ratio population is stationary and does not demonstrate time-dependent behavior, the summary statistics change over time. The Weibull distribution parameters fitted to the fifth-year report are utilized for the simulation. The shape and scale parameters of the Weibull distribution and their respective standard errors are shown in Table 6.

Lastly, the spatial distribution of pits on pipe surfaces is highly dependent on the environment. Despite the current data set being obtained from a buried pipeline where feature densities on pipe shoulders are more significant, it is chosen to adopt a uniform distribution for circumferential and axial spatial distributions. Considering this parameter only impacts the newly initiated corrosion pits, this approach does not impact the accuracy considerably as multiple instantiations of the surfaces will capture all possible interactions among the defects.

4.4. Simulation results

Using the input parameters obtained fromSections 4.1 to 4.3 and applying the approach discussed in 2.4, 10,000 instances of each of the 246 pipe joints are simulated. Utilizing the three standard practices for burst pressure assessment according to the procedures discussed in Section 2.5, the maximum allowable pressure of each instantiation of each pipe joint is calculated. The median of the estimated burst pressures of each pipe joint is then used to represent the simulation results in Fig. 13. The predicted burst pressures in ascending order of the calculation results obtained from RP-F101 are shown in Fig. 13.

Table 6
Pit length to depth ratio Weibull distribution parameters.

Shape	Shape Std. Err.	Scale	Scale Std. Err.
1.1	0.01	89.48	1.33

There are two aspects of this graph worthy of discussion concerning the impact of pit interaction criteria. The fluctuations observed in the assessments based on Z662 and B31G compared to F101 are signs of the impact of both interaction criteria and burst pressure assessment formulation. It can be observed that the fluctuations are more significant in Z662 due to the larger distance. On the other hand, the fluctuations observed in the assessment results when comparing the Z662 and B31G burst pressures are only the results of the interaction criteria. The use of various burst pressure assessment methods is motivated by the need to check consistency in results and compare the impact of interaction criteria. The consistency among the results, i.e., F101 being the least conservative and B31G the most, agrees with previous comparative studies (Hasan et al., 2011; Hasan et al., 2012; Liu et al., 2019).

Fig. 14 illustrates and summarizes the predictive performance of the proposed approach. Each subplot, a, b, or c visualizes the predictive performance when different burst pressure assessment methods are implemented. Furthermore, predictive performance using each burst pressure assessment approach is visualized using three plots. The wide plot on top illustrates the deviation of the predicted mean and 95% upper confidence interval (CI) from the calculated remaining strength of individual pipe joints based on the seventh-year inspection. As expected, the 95% upper CI results in smaller deviations; at the same time, being conservative, it underestimates the remaining strength of each joint in most cases. Additionally, the percentage prediction errors (Guang et al., 1995) for the median and the 95% interval compared to the estimated value are presented in the two graphs below the deviations. The percentage prediction error is calculated using Eq. (19).

$$\%Prediction\ Error = \frac{Measured\ Value - Predicted\ Value}{Measured\ Value} \times 100\% \tag{19}$$

The prediction error graphs visualize this property using the histogram and density curve of the distribution of errors. According to the prediction errors, we can see that both the median and the 95% upper CI demonstrate accuracies ranging between 2%–6% maximum, depending on the applied burst pressure calculation scheme. Judging from the density plots of the error distributions in all cases, it can be concluded that they are normally distributed.

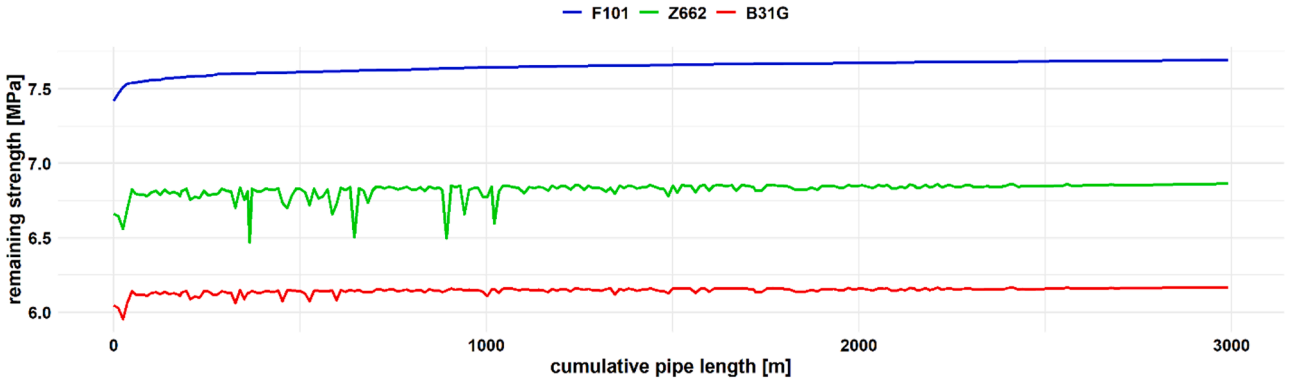

Fig. 13. The predicted burst pressures in ascending order based on F101 calculations.

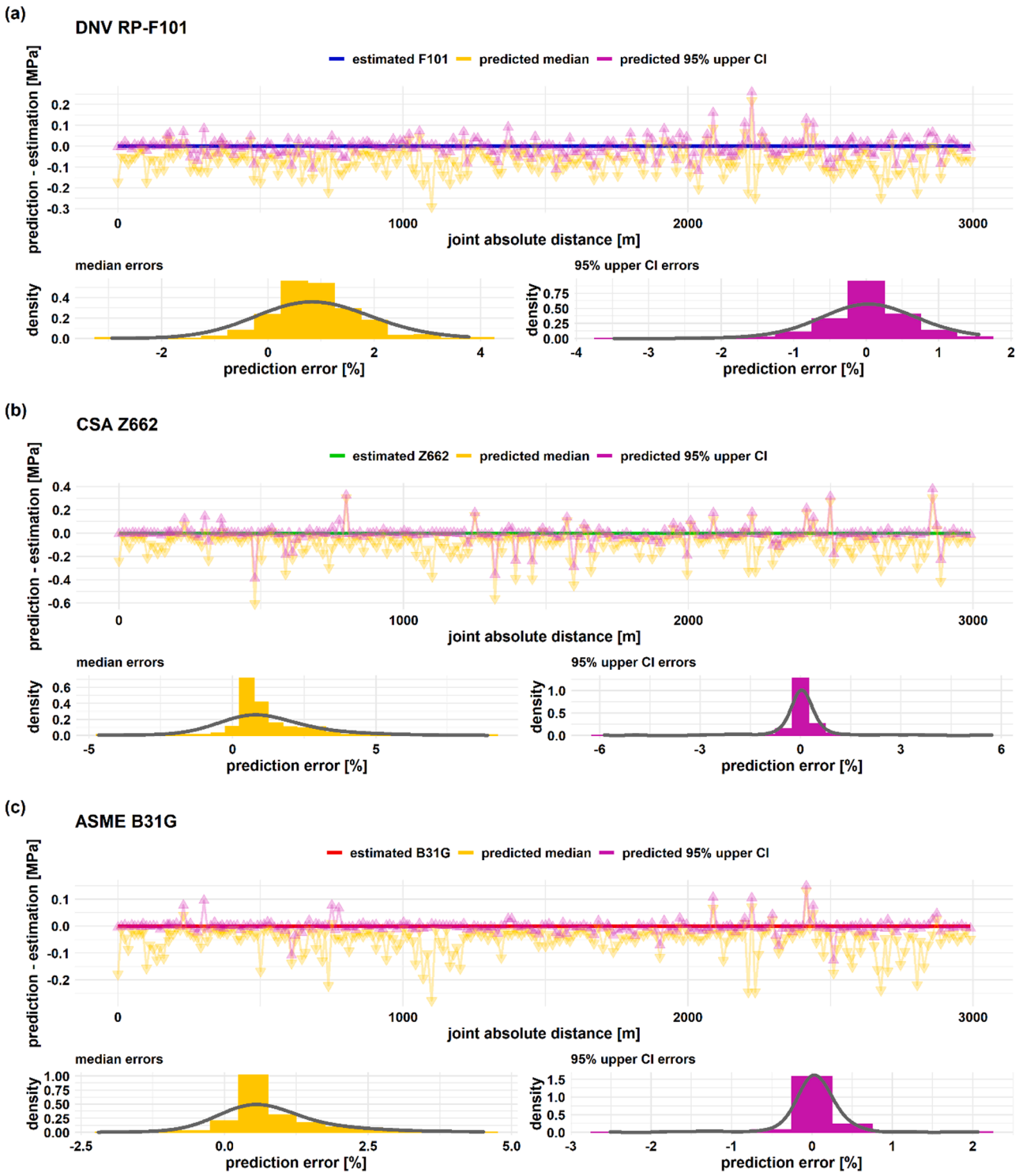

Fig. 14. Deviation of predicted failure pressure (MPa) mean and 95% upper interval on top, the predictive errors of the mean, and 95% upper CI on the bottom left and right, respectively calculated using (a) DNV RP F101, (b) CSA Z662, and (c) ASME B31G.

5. Conclusion

Even though the likelihood of pipe burst occurrence is many times less than the possibility of leakage (Valor et al., 2014), the potentially high consequences of such failures necessitate the development of viable predictive methods for this type of failure. It was mentioned that burst pressure assessment requires more information about the pipe surface, unlike leakage, where the only varying parameters are depth and pipe wall thickness. It was also mentioned that assessing pit interaction and dimensions is required. Considering the randomness of factors impacting interaction, i.e., pit location and dimensions, any predictive approach should approach this issue through probabilistic and stochastic approaches. Here a method is proposed to capture degradation paths, which allows data collection on damage progress by combining widely accepted stochastic degradation models. The estimated burst pressure based on the simulated surface shows great agreement with the burst pressure calculated according to the latest inspection data. Although dependent on the burst pressure calculation guidelines, the

prediction error is consistently below 6%, showing the simulation approach's capacity to predict degradation progress. Considering the positive mean of the errors, the simulation seems to result in conservative assessment predictions. Even though the insignificant conservativeness, in this case, does not have dire safety implications, further analysis is required to identify its source for future improvements. This approach shows great accuracy even though no error reduction methods were applied to the dataset. The satisfactory results suggest that the overall approach can accurately predict defect growth and the impact of pit interaction. A shortcoming of this study is the relatively short interval between the last report and the desired time in the case study, i.e., two years. These results from this short time horizon show potential for application in maintenance prioritization and inspection interval optimization. At the same time, the viability of this proposed method should be judged over long periods. Lastly, the proposed approach owes its versatility to its output, the remaining strength of sections regardless of the length. Therefore, it could be implemented as a complement to integrity management programs to assess fitness for service to manage the risks associated with operational pressures. Moreover, the high predictive accuracy of the approach in damage prediction down to sections as small as pipe joints provides an opportunity to improve the cost-effectiveness of maintenance and inspection activities.

Data availability statement

The filtered data supporting the findings of this article are openly available in Mendeley Data at http://dx.doi.org/10.17632/c2h2jf5c54.1 [66].

Declaration of Competing Interest

The authors declare that they have no known competing financial interests or personal relationships that could have appeared to influence the work reported in this paper.

Acknowledgments

The authors acknowledge the financial support provided by Genome Canada and their supporting partners and the Canada Research Chair (CRC) Tier I Program in Offshore Safety and Risk Engineering.

References

Adumene, S., Khan, F., Adedigba, S., 2020. Operational safety assessment of offshore pipeline with multiple MIC defects. Comput Chem Eng 138, 106819. https://doi.org/10.1016/j.compchemeng.2020.106819.

Alamilla, J.L., Sosa, E., 2008. Stochastic modelling of corrosion damage propagation in active sites from field inspection data. Corros Sci 50 (7), 1811–1819. https://doi.org/10.1016/j.corsci.2008.03.005.

Alfonso, L., Caleyo, F., Hallen, J.M., Araujo, J., 2010. On the applicability of extreme value statistics in the prediction of maximum pit depth in heavily corroded non-piggable buried pipelines 4, 527–535. https://doi.org/10.1115/IPC2010-31321.

API, 2019. Recommended Practice 1160 - Managing System Integrity for Hazardous Liquids Pipelines. American Petroleum Institute.

ASME, 2012. B31G - 2012(R2017) Manual for Determining the Remaining Strength of Corroded Pipelines. American Society of Mechanical Engineers.

ASME, 2018. B31.8S - Managing System Integrity of Gas Pipelines. American Society of Mechanical Engineers.

Aziz, P.M., 1956. Application of the statistical theory of extreme values to the analysis of maximum pit depth data for aluminum. Corrosion 12 (10), 35–46.

Burstein, G.T., Liu, C., Souto, R.M., Vines, S.P., 2004. Origins of pitting corrosion. Corrosion Engineering, Science and Technology 39 (1), 25–30.

Butler, G., Stretton, P., Beynon, J.G., 1972. Initiation and growth of pits on high-purity iron and its alloys with chromium and copper in neutral chloride solutions. British Corrosion Journal 7 (4), 168–173.

Cawley, N.R., Harlow, D.G., 1996. Spatial statistics of particles and corrosion pits in 2024-T3 aluminium alloy. J Mater Sci 31 (19), 5127–5134.

Coles, S., Bawa, J., Trenner, L., Dorazio, P., 2001. An Introduction to Statistical Modeling of Extreme Values, 208. Springer.

CSA, 2019. Oil and Gas Pipeline systems: CSA Z662:19. Canadian Standards Association, Toronto.

Dann, M.R., Maes, M.A., 2018. Stochastic corrosion growth modeling for pipelines using mass inspection data. Reliability Engineering & System Safety 180, 245–254. https://doi.org/10.1016/j.ress.2018.07.012.

Dey, D.K., Yan, J., 2016. Extreme Value Modeling and Risk analysis: Methods and Applications. CRC Press. Sci-hub.do books.google.ca/books?hl=en&lr=&id=PYhUCwAAQBAJ&oi=fnd&pg=PP1&dq=extreme+value+modeling+and+risk+analysis&ots=pjR170mlD1&sig=SxQqrr9-do2Y2PCf0YJAjiiob1Y.

DNV, 2019. DNV-RP-F101 : CORRODED PIPELINES. DET NORSKE VERITAS AS.

Gomes, W.J.S., Beck, A.T., Haukaas, T., 2013. Optimal inspection planning for onshore pipelines subject to external corrosion. Reliability Engineering & System Safety 118, 18–27. https://doi.org/10.1016/j.ress.2013.04.011.

Gong, C., Zhou, W., 2018. Importance sampling-based system reliability analysis of corroding pipelines considering multiple failure modes. Reliability Engineering and System Safety 169, 199–208. https://doi.org/10.1016/j.ress.2017.08.023.

Guang, W., Baraldo, M., Furlanut, M., 1995. Calculating percentage prediction error: a user's note. Pharmacol. Res. 32 (4), 241–248. https://doi.org/10.1016/S1043-6618(05)80029-5.

Hammersley, J.M., Handscomb, D.C., 1964. Monte Carlo Methods. Chapman and Hall, Ltd.

Hasan, M., Khan, F., Kenny, S., 2011. Identification of the Cause of Variability of Probability of Failure for Burst Models Recommended by Codes/Standards. J Press Vessel Technol 133 (4). https://doi.org/10.1115/1.4002862.

Hasan, S., Khan, F., Kenny, S., 2012. Probability assessment of burst limit state due to internal corrosion. International Journal of Pressure Vessels and Piping 89, 48–58. https://doi.org/10.1016/j.ijpvp.2011.09.005.

Heidary, R., Groth, K.M., 2021. A hybrid population-based degradation model for pipeline pitting corrosion. Reliability Engineering & System Safety 214, 107740. https://doi.org/10.1016/j.ress.2021.107740.

Khan, F., Yarveisy, R., Abbassi, R., 2021a. Risk-based pipeline integrity management: a road map for the resilient pipelines. Journal of Pipeline Science and Engineering 1 (1), 74–87. https://doi.org/10.1016/j.jpse.2021.02.001.

Khan, F., Yarveisy, R., Abbassi, R., 2021b. Cross-country pipeline inspection data analysis and testing of probabilistic degradation models. Journal of Pipeline Science and Engineering 1 (3), 308–320. https://doi.org/10.1016/j.jpse.2021.09.004.

Kiefner, J.F., Vieth, P.H., 1989. A modified criterion for evaluating the remaining strength of corroded pipe. Battelle Columbus Div.

Kiefner, J.F., Vieth, P.H., 1990. Evaluating pipe–1. new method corrects criterion for evaluating corroded pipe. Oil and Gas Journal 88 (32).

Kotz, S., Nadarajah, S., 2000. Extreme Value distributions: Theory and Applications. World Scientific.

Kroese, D.P., Brereton, T., Taimre, T., Botev, Z.I., 2014. Why the Monte Carlo method is so important today. WIREs Computational Statistics 6 (6), 386–392. https://doi.org/10.1002/wics.1314.

Larrosa, N.O., Lopez-Crespo, P., Ainsworth, R.A., 2018. An efficient procedure for reducing in-line-inspection datasets for structural integrity assessments. Theoretical and Applied Fracture Mechanics 93, 79–87. https://doi.org/10.1016/j.tafmec.2017.07.005.

Liu, A., Chen, K., Huang, X., Chen, J., Zhou, J., Xu, W., 2019. Corrosion failure probability analysis of buried gas pipelines based on subset simulation. J Loss Prev Process Ind 57, 25–33. https://doi.org/10.1016/j.jlp.2018.11.008.

Melchers, R.E., 2004. Pitting Corrosion of Mild Steel in Marine Immersion Environment—Part 1: maximum Pit Depth. Corrosion 60 (9), 824–836.

Melchers, R.E., 2005a. Statistical characterization of pitting corrosion - Part 1: data analysis. Corrosion 61 (7), 655–664.

Melchers, R.E., 2005b. Statistical characterization of pitting corrosion - Part 2: probabilistic modeling for maximum pit depth. Corrosion 61 (8), 766–777.

Melchers, R.E., 2008a. Corrosion wastage in aged structures. Condition Assessment of Aged Structures. https://doi.org/10.1533/9781845695217.2.77.

Melchers, R.E., 2008b. Extreme value statistics and long-term marine pitting corrosion of steel. Probabilistic Engineering Mechanics 23 (4), 482–488. https://doi.org/10.1016/j.probengmech.2007.09.003.

Melchers, R.E., 2010. Estimating uncertainty in maximum pit depth from limited observational data. Corrosion Engineering Science and Technology 45 (3), 240–248. https://doi.org/10.1179/147842209x12489567719581.

Melchers, R.E., 2015. Progression of pitting corrosion and structural reliability of welded steel pipelines. Oil and Gas Pipelines 327–342.

Mercer, A.D., Lumbard, E.A., 1995. Corrosion of mild steel in water. British Corrosion Journal 30 (1), 43–55.

Nessim, M., Mora, R., Dawson, J., Hassanein, S., 2009. Obtaining corrosion growth rates from repeat in-line inspection runs and dealing with the measurement uncertainties. Proceedings of the Biennial International Pipeline Conference, IPC 2, 593–600. https://doi.org/10.1115/IPC2008-64378.

Ossai, C.I., Boswell, B., Davies, I.J., 2015. Pipeline failures in corrosive environments - A conceptual analysis of trends and effects. Eng Fail Anal 53, 36–58. https://doi.org/10.1016/j.engfailanal.2015.03.004.

Pasupathy, R., 2010. Generating Homogeneous Poisson processes. Wiley Encyclopedia of Operations Research and Management Science.

PHMSA. (n.d.). *Pipeline Incident 20 Year Trends*. Retrieved November 20, 2021, from https://www.phmsa.dot.gov/data-and-statistics/pipeline/pipeline-incident-20-year-trends.

POF. (2021). *Standard Practice - POF 100: specifications and requirements for in-line inspection of pipelines.*

Rivas, D., Caleyo, F., Valor, A., Hallen, J.M., 2008. Extreme value analysis applied to pitting corrosion experiments in low carbon steel: comparison of block maxima and

peak over threshold approaches. Corros Sci 50 (11), 3193–3204. https://doi.org/10.1016/j.corsci.2008.08.002.
Sánchez, J.F., Alhama, F., Moreno, J.A., 2012. An efficient and reliable model based on network method to simulate CO2 corrosion with protective iron carbonate films. Comput Chem Eng 39, 57–64. https://doi.org/10.1016/j.compchemeng.2011.11.011.
Scarf, P.A., 1992. Extrapolation of Extreme Pit Depths in Space and Time Using the r Deepest Pit Depths. J Electrochem Soc 139 (9), 2621. https://doi.org/10.1149/1.2221275.
Shekari, E., Khan, F., Ahmed, S., 2016. A predictive approach to fitness-for-service assessment of pitting corrosion. International Journal of Pressure Vessels and Piping 137, 13–21. https://doi.org/10.1016/j.ijpvp.2015.04.014.
Shibata, T., 1996. ***1996 W.R. Whitney Award Lecture:*** statistical and Stochastic Approaches to Localized Corrosion. CORROSION 52 (11), 813–830. https://doi.org/10.5006/1.3292074.
Tak, K., Kim, J., 2018. Corrosion effect on inspection and replacement planning for a refinery plant. Computers and Chemical Engineering 117, 97–104. https://doi.org/10.1016/j.compchemeng.2018.05.027.
Tan, J.S., Kramer, M.A., 1997. A general framework for preventive maintenance optimization in chemical process operations. Comput Chem Eng 21 (12), 1451–1469. https://doi.org/10.1016/S0098-1354(97)88493-1.
Tsukaue, Y., Nakao, G., Takimoto, Y., Yoshida, K., 1994. Initiation Behavior of Pitting in Stainless Steels by Accumulation of Triiodide Ions in Water Droplets. CORROSION 50 (10), 755–760. https://doi.org/10.5006/1.3293465.
Uhlig, H.H., Revie, R.W., 1985. Corrosion and corrosion control.
Valor, A., Caleyo, F., Alfonso, L., Velázquez, J.C., Hallen, J.M., 2013. Markov chain models for the stochastic modeling of pitting corrosion. Mathematical Problems in Engineering 2013. https://doi.org/10.1155/2013/108386.
Valor, A., Caleyo, F., Alfonso, L., Vidal, J., Hallen, J.M., 2014. Statistical Analysis of Pitting Corrosion Field Data and Their Use for Realistic Reliability Estimations in Non-Piggable Pipeline Systems. CORROSION 70 (11), 1090–1100. https://doi.org/10.5006/1195.
Valor, A., Caleyo, F., Rivas, D., Hallen, J.M., 2010. Stochastic approach to pitting-corrosion-extreme modelling in low-carbon steel. Corros Sci 52 (3), 910–915. https://doi.org/10.1016/j.corsci.2009.11.011.
Valor, A., Rivas, D., Caleyo, F., Hallen, J.M., 2007. Discussion: statistical characterization of pitting corrosion - Part 1: data analysis and part 2: probabilistic modeling for maximum pit depth. Corrosion 63 (2), 107–113. https://doi.org/10.5006/1.3281683.
Vassiliadis, C.G., Pistikopoulos, E.N., 2001. Maintenance scheduling and process optimization under uncertainty. Comput Chem Eng 25 (2–3), 217–236. https://doi.org/10.1016/S0098-1354(00)00647-5.
Velázquez, J.C., Caleyo, F., Valor, A., Hallen, J.M., 2009. Predictive model for pitting corrosion in buried oil and gas pipelines. Corrosion 65 (5), 332–342. https://doi.org/10.5006/1.3319138.
Velazquez, J.C., Valor, A., Caleyo, F., Venegas, V., Espina-Hernandez, J.H., Hallen, J.M., Lopez, M.R., 2009. Study helps model buried pipeline pitting corrosion. Oil and Gas Journal 107 (27), 64–73. https://www.scopus.com/inward/record.uri?eid=2-s2.0-67651017917&partnerID=40&md5=942a35f65ed0d5d90ef251e3660dd6a4.
Xie, M., Tian, Z., 2018. A review on pipeline integrity management utilizing in-line inspection data. Eng Fail Anal 92 (May), 222–239. https://doi.org/10.1016/j.engfailanal.2018.05.010.
Yarveisy, R., Khan, F., Abbassi, R., 2022. Data-driven predictive corrosion failure model for maintenance planning of process systems. Comput Chem Eng 157, 107612. https://doi.org/10.1016/j.compchemeng.2021.107612.
Zhang, S., Zhou, W., 2014. Cost-based optimal maintenance decisions for corroding natural gas pipelines based on stochastic degradation models. Engineering Structures 74, 74–85. https://doi.org/10.1016/j.engstruct.2014.05.018.
Zhang, S., Zhou, W., Al-Amin, M., Kariyawasam, S., Wang, H., 2012. Time-dependent corrosion growth modeling using multiple ili data 4, 693–702. https://doi.org/10.1115/IPC2012-90502.
Zhou, W., Xiang, W., Hong, H.P., 2017. Sensitivity of system reliability of corroding pipelines to modeling of stochastic growth of corrosion defects. Reliability Engineering and System Safety 167 (January), 428–438. https://doi.org/10.1016/j.ress.2017.06.025.